

# One, two or three stars? An investigation of an unusual eclipsing binary candidate undergoing dramatic period changes

M. E. Lohr<sup>1</sup>, A. J. Norton<sup>1</sup>, U. C. Kolb<sup>1</sup>, and D. R. S. Boyd<sup>2</sup>

<sup>1</sup> Department of Physical Sciences, The Open University, Walton Hall, Milton Keynes MK7 6AA, UK  
e-mail: Marcus.Lohr@open.ac.uk

<sup>2</sup> The British Astronomical Association, Burlington House, Piccadilly, London W1J 0DU, UK

Received 26 July 2013 / Accepted 30 August 2013

## ABSTRACT

We report our investigation of 1SWASP J234401.81–212229.1, a variable with a 18 461.6 s period. After identification in a 2011 search of the SuperWASP archive for main-sequence eclipsing binary candidates near the distribution's short-period limit of  $\sim 0.20$  d, it was measured to be undergoing rapid period decrease in our earlier work, though later observations supported a cyclic variation in period length. Spectroscopic data obtained in 2012 with the Southern African Large Telescope did not, however, support the interpretation of the object as a normal eclipsing binary. Here, we consider three possible explanations consistent with the data: a single-star oblique rotator model in which variability results from stable cool spots on opposite magnetic poles; a two-star model in which the secondary is a brown dwarf; and a three-star model involving a low-mass eclipsing binary in a hierarchical triple system. We conclude that the latter is the most likely model.

**Key words.** stars: individual: 1SWASP J234401.81–212229.1 - stars: variables: general - binaries: close - binaries: eclipsing

## 1. Introduction

The object 1SWASP J234401.81–212229.1 (J2344) was identified as a candidate W UMa-type (contact) eclipsing binary in Norton et al. (2011), primarily on the basis of light curve shape. Using observations from the SuperWASP archive (Pollacco et al. 2006), a best period of 0.21367 d was found<sup>1</sup>, giving it immediate interest as being very close to the observed lower limit in the period distribution of main sequence binaries of  $\sim 0.2$  d (Rucinski 1992). Lohr et al. (2012) then found evidence of substantial period changes in J2344, which suggested rapid period decrease on the basis of the first four years of SuperWASP data, implying a stellar merger within 40 000 years at most. However in Lohr et al. (2013), which found the object's period as  $18\,461.639 \pm 0.0005$  s (0.21367638 d), more recently-available SuperWASP observations supported a subsequent increase in period: J2344 currently appears to be undergoing dramatic and approximately sinusoidal variations in period length.

Two other objects from the Lohr et al. (2013) collection of 143 SuperWASP candidate eclipsing binaries with periods below 20 000 s have since been followed up spectroscopically, and in spite of relatively low S/N spectra, were confirmed as low-mass double-lined spectroscopic and eclipsing binaries (paper submitted to A&A). Therefore, with high-resolution spectra, the prospects seemed good for confirming J2344 as a binary system, determining its parameters and identifying the cause of its period variation. Observations were made with the Southern African

Large Telescope (SALT) in mid-2012, from which we hoped to extract radial velocities for the system components. Moreover, additional photometric observations of J2344 were made during late 2012, with a view to measuring more recent eclipse timings.

Here we report the surprising results of the follow-up observations: that J2344 does not appear to be a straightforward eclipsing binary system. It remains a mysterious object, though certain explanations are supported by the data while others are ruled out. We consider three possible models, and identify one as most plausible on current evidence. Whatever the true nature of this object, it is hoped that this exploration will be of value for studies of low-mass stars and variables in general.

## 2. Observations

### 2.1. Photometry

The SuperWASP archive contains 21727 photometric points for J2344, obtained between 15 May 2006 and 2 August 2011. The fluxes, approximately corresponding to the Johnson V band, were corrected by Sys-Rem (Tamuz et al. 2005; Mazeh et al. 2006), and were extracted using a 3.5 pixel-radius photometric aperture (the middle of SuperWASP's three photometric apertures), corresponding to  $47''.95$ . Fig. 1 shows the local star field, including two nearby sources evaluated for their possible contribution to the observed SuperWASP light curve. Periods and period changes were measured using a custom IDL program, described in Lohr et al. (2013), resulting in a high-precision phase-folded light curve.

Additional photometric observations were made of J2344 and nearby sources by D. Boyd in the southern UK, for 0.5 h on 18 December and 1.1 h on 29 December 2012. A 0.35 m telescope with Starlight Xpress SXV-H9 CCD was used (pixel size  $12.9 \mu\text{m} = 1''.2$ ). On 18 December, the average FWHM was

<sup>1</sup> The corresponding object ASAS J234402–2122.5 found from ASAS observations is listed in the AAVSO International Variable Star Index as a W UMa-type eclipsing binary with a period of 0.2136764 d; in the ASAS Catalog of Variable Stars as a semi-detached eclipsing binary, period 0.213678 d; and in the Machine-learned ASAS Classification Catalog as a  $\delta$  Scuti pulsating variable with period 0.10684 d.

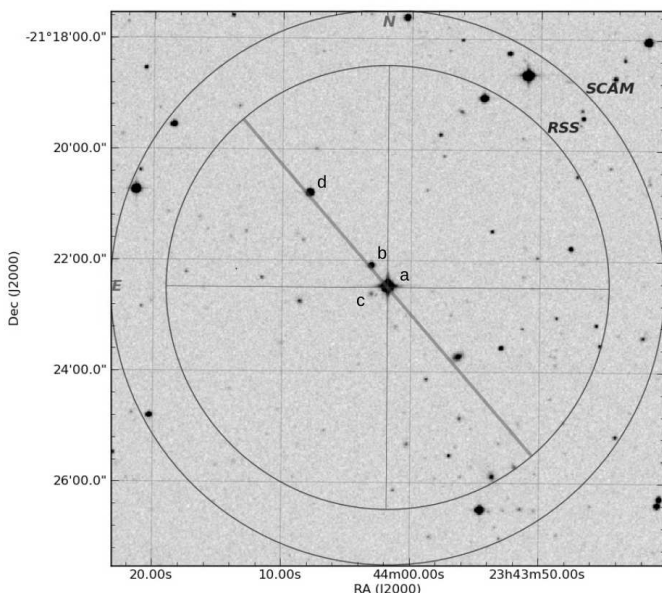


**Fig. 1.** Local star field of J2344 (a). The outer circle shows the field of view of the SALTICAM imager; the inner is that of the Robert Stobie Spectrograph (RSS). The diagonal line shows the angle of the spectrograph slit, chosen to include potential comparison stars b and d. Sources b and c would have fallen within the SuperWASP photometric aperture for J2344.

3'6, air mass 3.4, and exposure duration 30 s; on 29 December the corresponding values were 5'6, 5.7 and 60 s; both nights were affected by moonlight and low-altitude haze. One additional eclipse timing (HJD 2456291.33132) was determined, and the variability and magnitudes of several sources in the vicinity of J2344 were measured, using comparison stars GSC 06410-00829, GSC 06410-01027 and GSC 06410-00871 (magnitudes obtained from AAVSO APASS survey).

## 2.2. Spectroscopy

53 long-slit spectra were taken for J2344 according to an automated schedule, by duty astronomers at SALT (Buckley et al. 2006), using the PG1800 grating on the RSS (Burgh et al. 2003) on 1 June (16×60 s), 2 July (16×60 s), 1 August (4×60 s) and 3 August (16×60 s; 1×12 s). By chance there was substantial overlap in the phases covered by the second and fourth nights of observation; a total phase coverage of ~22% was achieved. The slit, with a width of 0'9, was intended to be aligned at 35.75° to capture two nearby stars for potential comparison with J2344 (see Fig. 1), but this was achieved to varying extents during the second, third and fourth nights, and not at all during the first night. A wavelength range of ~5800–7100 Å was covered, to include the Na I D doublet, H $\alpha$  and a large number of narrow metal lines characteristic of cool stars.

Primary reduction was carried out by the SALT pipeline, using the PySALT software package<sup>2</sup> (Crawford et al. 2010). This included fidelity checking, gain and cross-talk correction, overscan bias subtraction and amplifier mosaicking. Master bias subtraction is not suggested for SALT data; also, flat-fielding, cosmic-ray rejection and fringe subtraction were not implemented in the pipeline at the time, pending calibration. After initial attempts to use unflattened spectra, a master flat was con-

<sup>2</sup> <http://pysalt.salt.ac.za/>

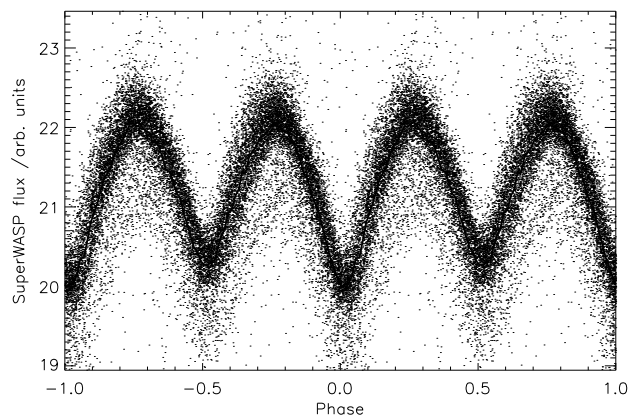


**Fig. 2.** SuperWASP light curve for J2344, folded at period of 18 461.639 s, with binned mean curve overplotted.

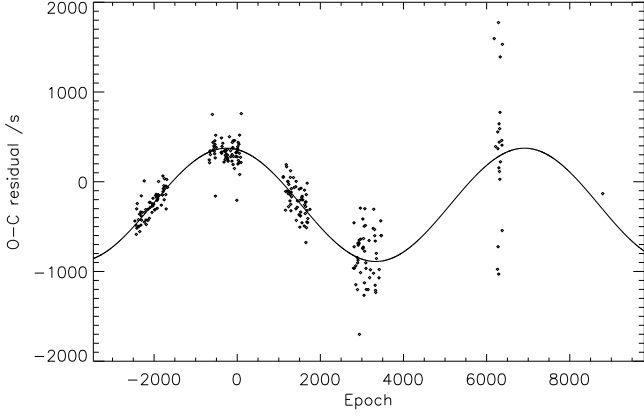
structed as a median of 10 flats supplied with the August spectra, and applied to all program images. Spectra were then optimally extracted using standard IRAF routines (which effectively cleaned out cosmic rays), and calibrated using neon arc lamp exposures. A resolution of ~0.41 Å per pixel was obtained.

In the apparent absence of visible line splitting or shifting in the spectra, no data-internal determination of phase was possible. Therefore phases were assigned to the spectra using a SuperWASP ephemeris in combination with D. Boyd's more recent eclipse timing. The source's spectral type was confirmed by cross-correlation using the IRAF task FXCOR, with comparison templates drawn from the Indo-U.S. Library of Coudé Feed Stellar Spectra (Valdes et al. 2004), which uses a comparable resolution (0.44 Å) and wavelength range (3460–9464 Å). Cross-correlation with a program spectrum of phase 0 was used to measure radial velocities (RVs), since the assumed two component spectra would be coincident during the primary eclipse.

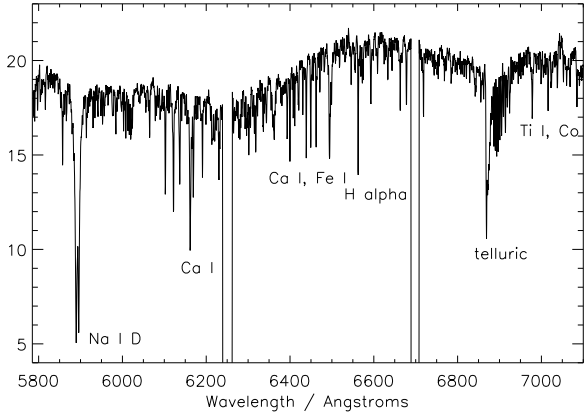
## 3. Results

Fig. 2 shows J2344's light curve, folded at its optimal period of 18 461.639 s. There is a small but consistent difference in the depths of primary and secondary minima, and continuous light variation, explaining its preliminary identification as an eclipsing binary in thermal contact. However, we may note the small amplitude of variation relative to the maximum or 'out-of-eclipse' flux level of ~22 units (~11.6 V mag): only about 1/11 of the light is lost during the assumed primary eclipse. This would imply a low angle of inclination of the system, a low mass ratio, and/or a third light entering the aperture.

Lohr et al. (2013) discusses the period changes we observed in J2344, and its Figs. 5 and 6 illustrate the best linear and quadratic fits to the data. The first four years suggested a rapid period decrease (reflected in an O–C parabola opening downwards), but the most recent year of SuperWASP data conflicted with this model ( $\chi^2 = 17.83$ ); assuming a half-cycle error in the primary minimum fits of the final year's data improved the quadratic fit ( $\chi^2 = 10.86$ ) but left Year 4 now visibly discrepant. Here, Fig. 3 gives the best sinusoidal fit to the SuperWASP data and the additional observation of a primary minimum from 2012; this provides an optimal model ( $\chi^2 = 2.82$ ), and suggests a meta-period for J2344 of  $4.19 \pm 0.04$  years, with an amplitude of  $631 \pm 11$  s. The observed times of minima are listed in Table 2.



**Fig. 3.** O–C diagram for J2344, following subtraction of best linear fit. Best sinusoidal fit is overplotted (meta-period 4.19 y;  $\chi^2 = 2.82$ ). Uncertainties on individual points are not shown for clarity, but are typically of the order of  $\pm 100$  s. The final point, around epoch 9000, corresponds to the independent observation of D. Boyd, and has an uncertainty of  $\pm 60$  s.



**Fig. 4.** SALT spectrum at phase 0.588. The gaps around 6250 and 6700 Å correspond to the boundaries of the three CCDs.

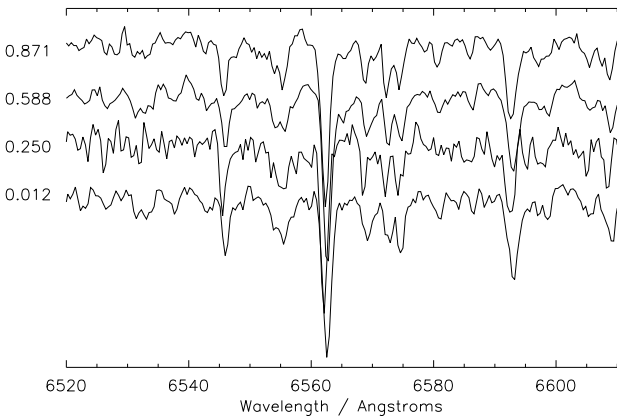


**Fig. 5.** Sections of SALT spectra around  $H\alpha$  line at 6562.8 Å, selected from the four nights of observation, and covering as wide a phase range as possible (phases shown on left).

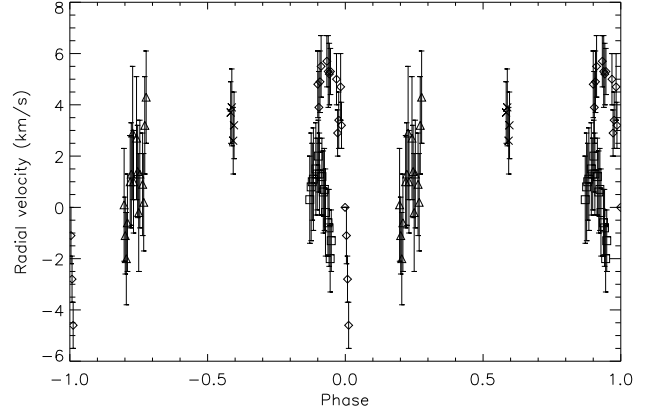


**Fig. 6.** RV curve for J2344. First night’s observations are plotted with triangles; second night: squares; third night: crosses; fourth night: diamonds.

Fig. 4 shows an example full extracted and calibrated spectrum for J2344. The best-matching comparison spectra were around K5V (temperatures between 4000 and 4500 K), achieving cross-correlation peak heights in excess of 0.95. However, to our surprise, little to no splitting or even shifting of the many well-defined absorption lines observed was apparent to the eye, as would be expected in a close, short-period eclipsing binary (Fig. 5). Only for spectra near phase 0.25 is there any suggestion of a leftward shift, and unfortunately, these spectra are by far the faintest of all four sets of observations, reducing their reliability. Moreover, an approximate light curve extracted from the spectra themselves (by fitting a spline to each continuum and evaluating it at a given wavelength) did not reflect the SuperWASP light curve at all, being apparently dominated by systematic effects.

Table 1 gives the heliocentric times, estimated phases and RVs for J2344’s spectroscopic observations. Only one clear cross-correlation peak was seen for each spectrum, rather than the two that we would expect for an eclipsing binary. (Repetition of the measurements using a template K5V spectrum produced very similar results, apart from a systematic offset due to relative centre-of-mass system velocities.) Fig. 6 plots the resulting RV curve against phase. We may note that the amplitude of variation is very small: only  $\pm 5$  km s<sup>-1</sup>, where we might expect values of tens or hundreds of km s<sup>-1</sup>. Also, such trends as are suggested over the orbital cycle do not seem to correspond to expected velocity changes for either component of a spectroscopic binary: some sort of maximum appears around phase 0.9 during the region of overlapping phase coverage, but this is when we expect the primary’s RV to be decreasing, and the secondary’s to be increasing; phase 0.25 should correspond to the primary’s minimum RV and the secondary’s maximum, but actually shows a rising trend in our plot.

#### 4. Discussion

Our spectroscopic results were not as expected given the photometric data for J2344. Its SuperWASP light curve (and indeed, the ASAS light curve of the corresponding source) strongly suggests a very short period eclipsing binary in contact configuration, like those of 1SWASP J150822.80–054236.9 and 1SWASP J160156.04+202821.6, which were recently confirmed as spectroscopic double-lined and eclipsing binaries, on the basis of fairly low-resolution INT spectra, and modelled as

**Table 1.** Summary of spectroscopic observations and RVs for J2344

HJD -2450000	Phase	RV (km s <sup>-1</sup> )	$\delta$ RV (km s <sup>-1</sup> )	HJD -2450000	Phase	RV (km s <sup>-1</sup> )	$\delta$ RV (km s <sup>-1</sup> )
6079.6205	0.197	0.1	2.2	6110.5461	0.928	-0.2	1.7
6079.6214	0.201	-1.1	1.5	6110.5480	0.937	-0.6	1.3
6079.6222	0.205	-2.0	1.8	6110.5489	0.941	-0.8	1.5
6079.6231	0.209	-0.6	1.9	6110.5498	0.945	-2.0	1.3
6079.6252	0.219	1.0	1.8	6110.5506	0.949	-1.3	1.2
6079.6261	0.223	1.3	2.0				
6079.6270	0.228	2.9	2.6	6141.4557	0.584	3.7	1.2
6079.6278	0.231	1.0	2.0	6141.4566	0.588	3.9	1.5
6079.6300	0.242	2.7	2.4	6141.4575	0.593	2.6	1.3
6079.6309	0.246	1.4	1.8	6141.4583	0.596	3.2	1.3
6079.6317	0.250	-0.2	2.3				
6079.6326	0.254	1.3	2.1	6143.4463	0.900	4.8	1.3
6079.6348	0.264	0.9	2.0	6143.4471	0.904	3.9	1.4
6079.6357	0.268	0.2	1.9	6143.4480	0.908	4.9	1.2
6079.6366	0.272	3.2	1.9	6143.4489	0.912	5.5	1.2
6079.6375	0.277	4.3	1.8	6143.4534	0.933	5.7	1.0
				6143.4543	0.938	5.3	1.4
6110.5340	0.871	0.3	1.7	6143.4552	0.942	5.2	1.2
6110.5349	0.876	0.8	2.1	6143.4560	0.946	5.3	0.9
6110.5358	0.880	1.0	1.5	6143.4607	0.968	5.0	1.0
6110.5367	0.884	1.1	2.0	6143.4616	0.972	2.9	0.9
6110.5387	0.893	1.5	1.8	6143.4625	0.976	3.4	1.1
6110.5396	0.898	1.3	1.4	6143.4640	0.983	4.7	1.3
6110.5405	0.902	2.0	1.4	6143.4647	0.986	3.2	0.9
6110.5413	0.906	1.3	1.6	6143.4675	0.999	0.0	0.0
6110.5434	0.915	1.2	1.5	6143.4684	0.004	-1.1	1.1
6110.5443	0.920	0.6	1.6	6143.4693	0.008	-2.8	0.9
6110.5452	0.924	0.7	1.6	6143.4702	0.012	-4.6	0.9

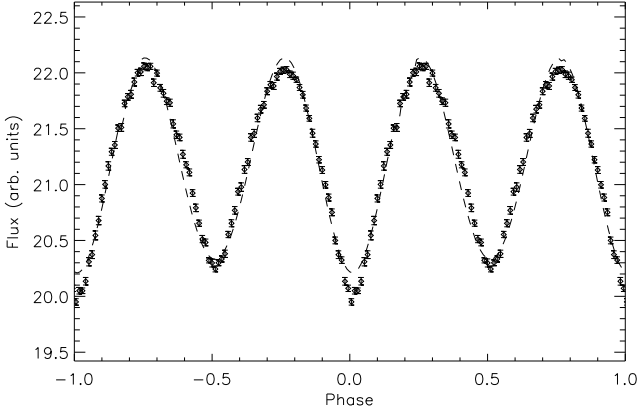


**Fig. 7.** Best light curve fit for PHOEBE model 1 of eclipsing binary assuming primary has mass consistent with K5V star, and secondary is massive enough to burn hydrogen ( $i = 44^\circ$ ,  $q = 0.11$ ,  $M_1 = 0.73M_\odot$ ,  $M_2 = 0.08M_\odot$ ). Binned input SuperWASP light curve shown with diamonds and uncertainty bars; fit with dotted line.

contact systems (paper submitted to A&A). However, the SALT spectra for J2344 showed little to no evidence for line splitting or shifting, being instead strongly consistent with a single, stable mid-K star.

To confirm our impression of the inconsistency of the photometric and spectroscopic results, modelling was carried out using the eclipsing binary modelling software PHOEBE (Prša & Zwitter 2005), built upon the code of Wilson & Devinney (1971). Figs. 7 to 10 illustrate the best light

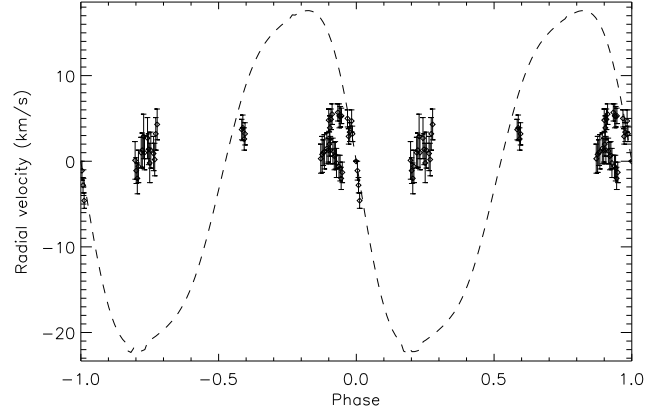


**Fig. 8.** Best primary RV curve fit for PHOEBE model 1 (parameters as for Fig. 7). SALT RV curve shown with diamonds and uncertainty bars; fit with dotted line.

curve and RV curve fits for two models: one optimising light curve fit and the second optimising RV curve fit. Input parameters of semi-major axis and mass ratio were constrained by the requirements that the more massive star in the assumed binary be consistent with a K5V spectrum, and its companion be massive enough to burn hydrogen, so that the system contains two main sequence stars. It may be seen that, with the minimum mass ratio  $q = 0.11$ , the observed light curve can be tolerably reproduced with a moderate angle of inclination  $i = 44^\circ$  (Fig. 7), but the corresponding primary RVs are then about three times larger than observed (Fig. 8). However, if  $i$  is reduced far enough to bring the modelled RV curve into the observed range (Fig. 10), the

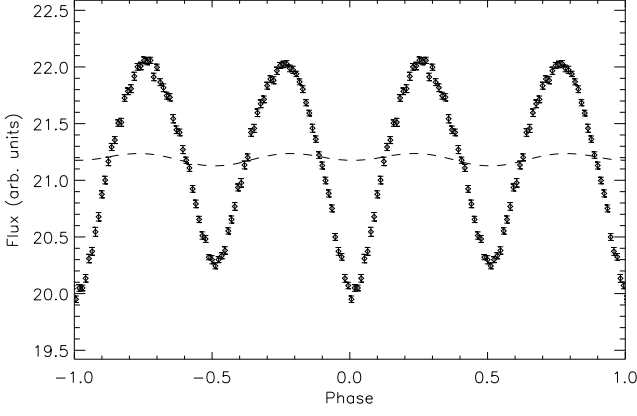


**Fig. 9.** Best light curve fit for PHOEBE model 2 of eclipsing binary assuming primary has mass consistent with K5V star, and secondary is massive enough to burn hydrogen ( $i = 10^\circ$ ,  $q = 0.11$ ,  $M_1 = 0.73M_\odot$ ,  $M_2 = 0.08M_\odot$ ).

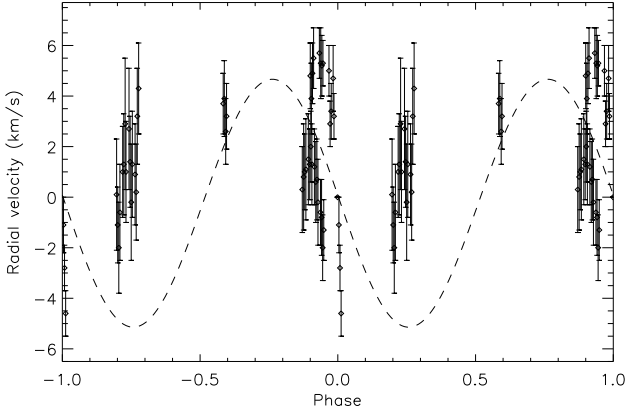


**Fig. 10.** Best primary RV curve fit for PHOEBE model 2 (parameters as for Fig. 9).

corresponding light curve model has far too small an amplitude (Fig. 9). Higher mass ratios fail to reproduce either light curve or RV curve, at any angle of inclination. Therefore we conclude that the observed photometry and spectroscopy, taken together, are incompatible with any low-mass eclipsing binary composed of main sequence stars.

One initial explanation considered was that J2344 was not in fact the source of the light variability observed by SuperWASP (and ASAS). Objects b and c, shown in Fig. 1, are close enough to J2344 to have fallen within the same SuperWASP photometric aperture. Could one of these be the expected eclipsing binary? Object b was captured within the SALT slit during three nights of observations, so its spectrum was also extracted and reduced. Although much fainter and noisier than J2344’s spectrum, the strongest absorption lines ( $H\alpha$  and  $Na\ I\ D$ ) were consistently visible, but showed no signs of shifting or splitting. Also, the SuperWASP archive contains a light curve for object b (1SWASP J234403.11-212205.8) which we obtained and analysed; in the 3.5 pixel aperture it showed similar variability to J2344, but in the smaller 2.5 pixel aperture, which should have excluded most of its neighbour’s flux, its variability was less periodic, while J2344’s light curve exhibited the same periodic behaviour even in the small aperture. Finally, D. Boyd con-

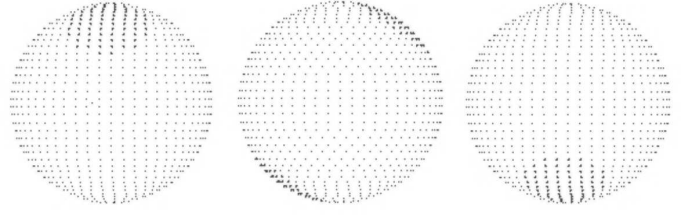


**Fig. 11.** PHOEBE images of spotted star model at phases 0.0, 0.25 and 0.5, from left to right.

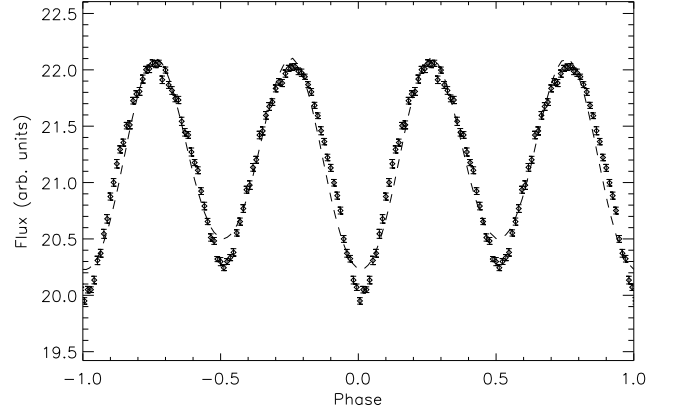


**Fig. 12.** Best light curve fit for PHOEBE spotted star model.

firmed from his 18 December 2012 observations of the field of view that object b had an (unfiltered) magnitude of  $15.46 \pm 0.21$ , corresponding to a SuperWASP flux variation of only about  $\pm 0.3$  units: far smaller than J2344’s amplitude of  $\pm 1$  unit. He also noted that object c did not surpass his sky background level of 16.5–17.0 mag; it therefore would have been too faint to be detectable by SuperWASP, with its range of  $\sim 8$ –15 V mag. We must conclude, then, that J2344 really is the source of the periodic photometric variation observed.

What, then, might explain an object with the light curve of a short-period binary but the spectrum of a single star? Moreover, what is the source of its dramatic period changes, with their 4.19 y meta-cycle? We have explored three physical models which provide potential explanations for these observations.

#### 4.1. One-star model

Our first model regards J2344 as what its spectrum indicates: a single mid-K dwarf, rotating with a period of 18 461.6 s. The low amplitude of light curve variability would be consistent with rotational variation caused by cool surface spots. However, the alternating deeper and shallower minima at phases 0.0 and 0.5 (Fig. 2), observed over many years of ASAS and SuperWASP data, would require two large stable spots of different areas and/or temperatures, located on diametrically-opposite sides of the star (Fig. 11). This could be achieved if the spots were somehow pinned to the star’s magnetic poles (Harrison et al. (2012) claimed similar cool stable polar spots on many K-class rotational variables observed with Kepler), and if the star were an oblique rotator (Stibbs 1950), having its magnetic axis at an angle to its axis of rotation. The small RV excursions from zero would then be caused by a form of the Rossiter-McLaughlin effect (Rossiter 1924; McLaughlin 1924) associated with the

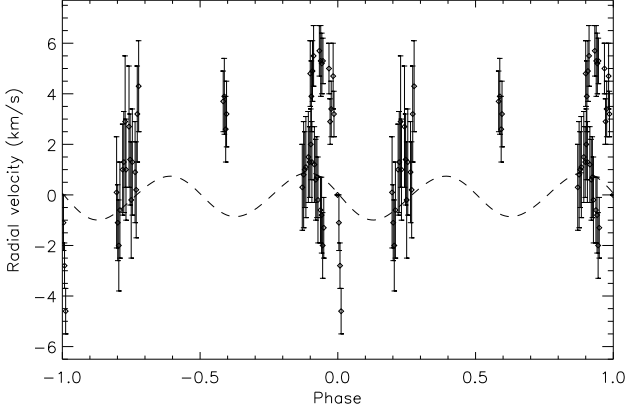


**Fig. 13.** Best RV curve fit for PHOEBE spotted star model.

spots, as observed by Huber et al. (2009). Precession due to the different alignments of magnetic and rotational axes might explain the 4.19 y meta-cycle of period changes (Monaghan 1968).

Using PHOEBE again to test this idea, we modelled a single rotational variable in similar fashion to Harrison et al., setting the input orbital period to the assumed rotational period and turning off the light from the detached companion. Since we were interested in reproducing the RVs as well as the light curve, we set the mass ratio as low as possible so that the modelled curves were both flat before the introduction of spots. The (primary) star was given a mass and effective temperature consistent with a K5V spectrum, and  $i$  was set to  $90^\circ$  for simplicity. Two spots were then added to the primary in accordance with the model, and adjusted manually until reasonable light and RV curve fits were obtained. The final spot location parameters were colatitudes  $35^\circ$  and  $145^\circ$  and longitudes  $0^\circ$  and  $180^\circ$  respectively, to simulate stable location on the poles of a magnetic axis at  $35^\circ$  to the rotational axis. One was given a slightly larger radius ( $26^\circ$  vs.  $25^\circ$ ) to reproduce the different depths of light curve minima, but both were set to the same temperature (20% of average).

Figs. 12 and 13 show the resulting fits. The light curve is fairly well reproduced, both in amplitude and different minima depths. The fitted RV curve is somewhat smaller in amplitude than that observed, but does match some of the velocity trends in the observed curve, notably the maximum around phase 0.9 and the rising trend around phase 0.25. Better fits might be obtained by modelling non-spherical spots, but these initial results may at least serve as proof of concept. A greater problem for the one-star model is the lack of evidence (to our knowledge) for other low-mass oblique rotators.

#### 4.2. Two-star model

Our second model for J2344 takes the light curve at face value, seeing it as an eclipsing binary in contact configuration, with a mid-K dwarf as primary, and a secondary component making a very limited contribution to the spectrum. In order to reproduce the observed amplitude of RV variation (associated with the primary, in this model), the secondary's mass must be in the brown dwarf range (Fig. 14). The observed shape of the RV curve would then be due to the Rossiter-McLaughlin effect as the secondary obscures each side of the primary in turn, and the 4.19 y meta-cycle of period changes could be explained by the Applegate mechanism (Applegate 1992).

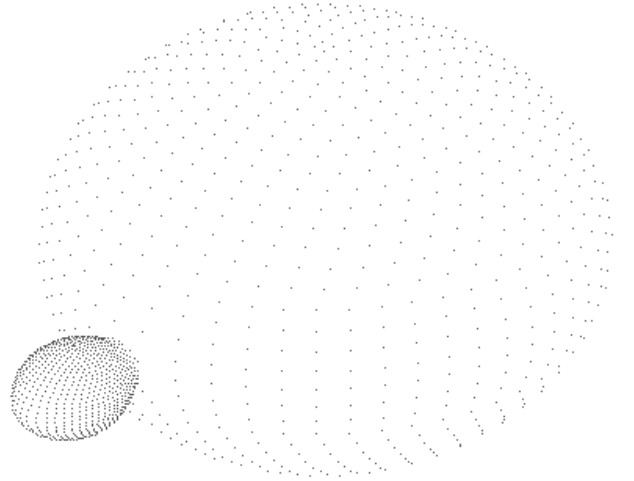


**Fig. 14.** PHOEBE image of K dwarf+brown dwarf binary model at phase 0.9.

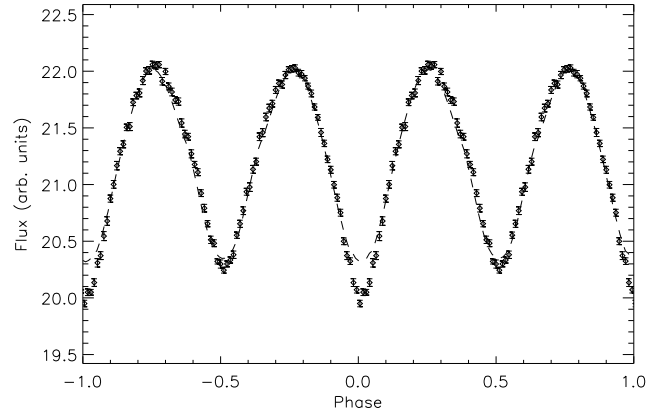


**Fig. 15.** Best light curve fit for PHOEBE K dwarf+brown dwarf binary model.

A PHOEBE model with  $i = 59^\circ$ ,  $q = 0.025$ ,  $M_1 = 0.79M_\odot$  and  $M_2 = 0.02M_\odot$  produced an excellent fit to the observed light curve amplitude and shape, though the different depths of minima could not be easily reproduced (Fig. 15). The RV fit (Fig. 16) was of slightly greater amplitude than the observed curve, but its Rossiter-McLaughlin effect-induced variations matched the velocity trends reasonably well, as with the spotted star model. We note, however, that PHOEBE is not intended to model planetary-mass companions, and may not model well objects in the brown dwarf range either, so these model outputs should be regarded with caution.

#### 4.3. Three-star model

Our final model for J2344 is of a triple system, consisting of a very low-mass contact eclipsing binary orbiting a more massive mid-K star which dominates the spectrum and obscures the contribution from the binary. The light curve is then the sum of a constant flux contribution from the K star (providing up to 9/11 of the maximum system flux), and a periodically-variable contribution from the binary. The radial velocity curve is almost constant, since it largely represents the unvarying (on this timescale)

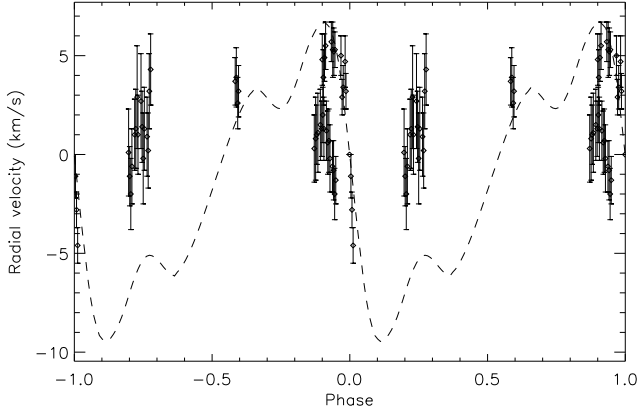


**Fig. 16.** Best primary RV curve fit for PHOEBE K dwarf+brown dwarf binary model.

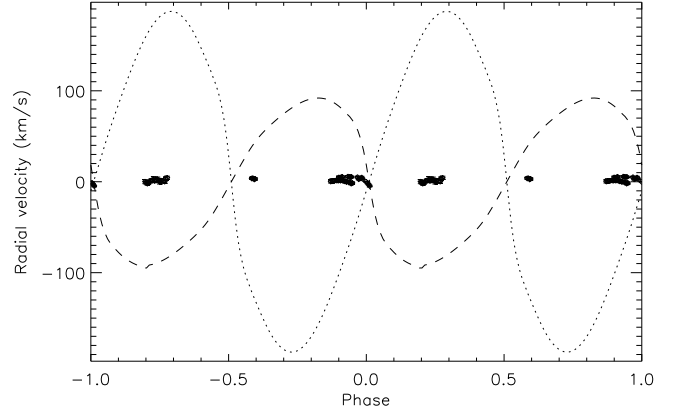


**Fig. 19.** RV curves corresponding to best light curve fit for PHOEBE M+M dwarf binary model (primary curve shown with dashed line; secondary with dotted line.)

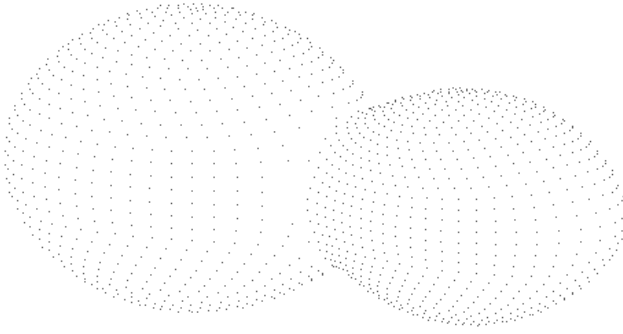


**Fig. 17.** PHOEBE image of M+M dwarf binary model at phase 0.15.

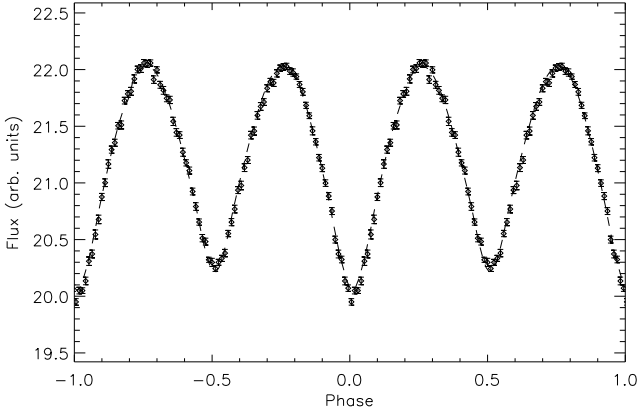


**Fig. 18.** Best light curve fit for PHOEBE M+M dwarf binary model.

position of the K dwarf. The 4.19 y cycle of period variation would be a light-time effect (LITE) resulting from the orbit of the contact binary around the most massive component of the triple.

A third light can be readily included in PHOEBE’s models; Figs. 17 to 19 show the results of modelling the eclipsing binary in such a triple system, using parameters  $i = 77^\circ$ ,  $q = 0.5$ ,  $M_1 = 0.34M_\odot$  and  $M_2 = 0.17M_\odot$  (i.e. M dwarfs), and a max-

imal third light of 18.0 SuperWASP flux units (11.86  $V$  mag). Fig. 17 indicates the very deep contact required; assuming this, however, an excellent fit to the light curve is achieved, without even needing spots to be included for fine-tuning (Fig. 18). Fig. 19 shows the primary and secondary RV curves implied for such an eclipsing binary, for reference only, since our observed SALT velocities are expected to be dominated by the constant K star, which is not included in the PHOEBE model as a mass, only as a light source.

Using these masses, totalling  $\sim 0.5M_\odot$ , for the binary, and a plausible  $0.65M_\odot$  for the K5 system primary, a binary-to-primary flux ratio of about 1:5 is implied, consistent with the modelled ratio of around 1:6 given by the SuperWASP light curve with maximum third light. We can also insert these values into the approximate formula for expected LITE changes for a binary in an edge-on circular orbit with a third body, given by Pribulla et al. (2012) in their Eq. 5:

$$\Delta T \approx \frac{2M_3G^{1/3}}{c} \left[ \frac{P_3}{2\pi(M_1 + M_2)} \right]^{2/3}, \quad (1)$$

where  $M_{1,2}$  are the masses of the binary components,  $M_3$  is the mass of the K5 system primary,  $P_3$  is the 4.19 y period of  $O - C$  oscillations, and  $\Delta T$  is the peak-to-peak amplitude of the  $O - C$  variations. The result is 2640 s, about twice the observed amplitude (Fig. 3), which is entirely plausible if we do not expect the angle of inclination to be  $90^\circ$ . (Indeed, using Pribulla et al.’s Eq. 10 with these masses and our observed semi-amplitude of LITE of 631 s,  $i = 56^\circ$  is suggested.)

On the assumption that this model was approximately correct, a suitably-scaled constant K5 template spectrum was subtracted from each of our spectra to see whether some trace of an M+M eclipsing binary spectrum might be detectable in the residuals. Fig. 20 shows the resulting RV curves, after cross-correlation with a phase 0 residual spectrum. A second cross-correlation peak was now marginally detectable in the spectra near quadrature, yielding RVs in a similar range, and following a similar upward trend, to those predicted for the primary curve in Fig. 19 near phase 0.25. The other RVs reached greater amplitudes than before (Fig. 6) and might conceivably represent a blending of lines from multiple stellar components. Given that our best model for the low-mass eclipsing binary in this putative triple system involves very deep contact, it is likely that their lines would be significantly broadened and blended even if no

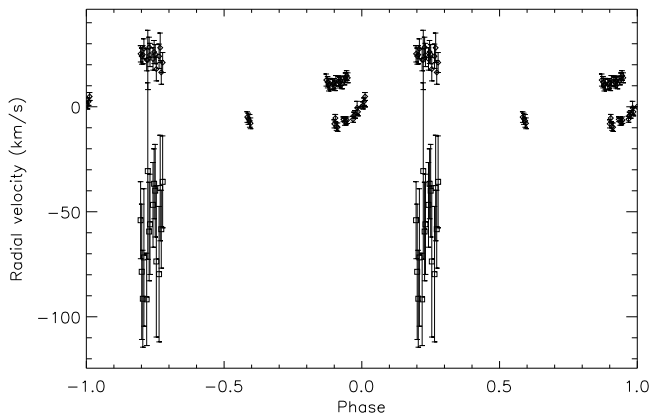


**Fig. 20.** Residual RV curves for J2344, following subtraction of scaled K5V template spectrum, and cross-correlation with phase 0 residual spectrum. The stronger cross-correlation peak velocities are shown with diamonds; the fainter cross-correlation peak visible near quadrature is plotted with squares.

third spectrum were present to complicate the picture, making extraction of RVs challenging in any case.

2MASS and WISE colours for the source were also checked for evidence of an infrared excess which might support the presence of M dwarfs in the system. The results were inconclusive, however: 2MASS J–H and H–K colours were in ranges expected for a K5 star, while the WISE colours were inconsistent, possibly being contaminated by nearby sources.

Although we lack conclusive evidence for it, a triple system seems the most likely of our three models for J2344. We have not assessed the dynamical stability of such a triple, but note the recent detection of a young hierarchical triple composed of a late-K primary and a pair of mid-M dwarfs in wide orbits (Deacon et al. 2013) which shows some similarity to the system posited here. Using the observed and theoretical absolute magnitudes for the stars in this model, a distance of 80–90 pc is indicated. The calculated separation between system primary and contact binary is 2.7 AU, which would then correspond to an angular separation of  $\sim 0''.03$ , making the components resolvable in principle. The expected RV amplitude for the system primary, over a 4.19 y orbital period with the binary, would be around  $8 \text{ km s}^{-1}$  (assuming a circular orbit and the same angle of inclination as for the contact binary), which might also be detectable in the long term.

## 5. Conclusions

Object J2344, which we originally thought might be an eclipsing binary close to stellar merger, has proved to be unusual and intriguing in a different way. Of the three models investigated here, a triple system containing a low-mass eclipsing binary appears the most plausible explanation for the apparently conflicting photometric and spectroscopic data, and provides an appealing reason for the dramatic cyclic variations in period length observed as well. If confirmed, it should provide a useful contribution to studies of multiple systems, alongside the quadruple doubly-eclipsing system already detected in our collection of short-period SuperWASP eclipsing binary candidates (Lohr et al. 2013).

Alternatively, if one of our other explanations proves more likely, J2344 could add to our knowledge of brown dwarfs, or

constitute a rare type of rotational variable. Still other explanations are no doubt conceivable e.g. involving higher multiplicity of the system; in any case, this appears to be an interesting object worthy of further observation. We would hope in the future to obtain multi-colour photometry and near-infrared spectroscopy of J2344, with improved phase coverage, in the expectation that the greater contrast available at longer wavelengths would increase the opportunity of detecting cool, low-mass objects within the system.

*Acknowledgements.* The WASP project is funded and operated by Queen’s University Belfast, the Universities of Keele, St. Andrews and Leicester, the Open University, the Isaac Newton Group, the Instituto de Astrofísica de Canarias, the South African Astronomical Observatory and by STFC. Some of the observations reported in this paper were obtained with the Southern African Large Telescope (SALT) under program 2012-1-UKSC-007 (PI: Andrew Norton). This work was supported by the Science and Technology Funding Council and the Open University.

## References

- Applegate, J. H. 1992, *ApJ*, 385, 621  
 Buckley, D. A. H., Swart, G. P., & Meiring, J. G. 2006, in *Ground-based and Airborne Telescopes*, ed. L. M. Stepp, Vol. 6267, 32  
 Burgh, E. B., Nordsieck, K. H., Kobulnicky, H. A., et al. 2003, in *Instrument Design and Performance for Optical/Infrared Ground-based Telescopes*, ed. M. Iye & A. Moorwood, Vol. 4841, 1463–1471  
 Crawford, S. M., Still, M., Schellart, P., et al. 2010, in *Observatory Operations: Strategies, Processes, and Systems III*, ed. D. R. Silva, A. B. Peck, & B. T. Soifer, Vol. 7737, 54  
 Deacon, N. R., Schlieder, J. E., Olofsson, J., Johnston, K. G., & Henning, T. 2013, *ArXiv e-prints*, 1306.2637  
 Harrison, T. E., Coughlin, J. L., Ule, N. M., & López-Morales, M. 2012, *ApJ*, 143, 4  
 Huber, K. F., Wolter, U., Czesla, S., et al. 2009, *A&A*, 501, 715  
 Lohr, M. E., Norton, A. J., Kolb, U. C., et al. 2012, *A&A*, 542, A124  
 Lohr, M. E., Norton, A. J., Kolb, U. C., et al. 2013, *A&A*, 549, A86  
 Mazeh, T., Tamuz, O., Zucker, S., et al. 2006, in *Tenth Anniversary of 51 Peg-b: Status of and prospects for hot Jupiter studies. Colloquium held at Observatoire de Haute Provence, France, August 22-25, 2005*, ed. L. Arnold, F. Bouchy, & C. Moutou (Paris: Frontier Group), 165–172  
 McLaughlin, D. B. 1924, *ApJ*, 60, 22  
 Monaghan, J. J. 1968, *Zeitschrift für Astrophysik*, 69, 154  
 Norton, A. J., Payne, S. G., Evans, T., et al. 2011, *A&A*, 528, A90  
 Pollacco, D. L., Skillen, I., Cameron, A. C., et al. 2006, *PASP*, 118, 1407  
 Pribulla, T., Vaňko, M., von Eiff, M. A., et al. 2012, *Astron. Nachr.*, 333, 754  
 Prša, A. & Zwitter, T. 2005, *ApJ*, 628, 426  
 Rossiter, R. A. 1924, *ApJ*, 60, 15  
 Rucinski, S. M. 1992, *AJ*, 103, 960  
 Stibbs, D. W. N. 1950, *MNRAS*, 110, 395  
 Tamuz, O., Mazeh, T., & Zucker, S. 2005, *MNRAS*, 356, 1466  
 Valdes, F., Gupta, R., Rose, J. A., Singh, H. P., & Bell, D. J. 2004, *ApJS*, 152, 251  
 Wilson, R. E. & Devinney, E. J. 1971, *ApJ*, 166, 605



**Table 2.** Times of primary eclipses for J2344.

Epoch	Heliocentric Julian Date	Uncertainty (days)
-2461	2453886.60695	0.00072
-2433	2453892.58935	0.00069
-2428	2453893.65657	0.00107
-2419	2453895.58295	0.00267
-2414	2453896.64885	0.00093
-2405	2453898.57511	0.00139
-2377	2453904.55514	0.00267
-2372	2453905.62436	0.00085
-2363	2453907.54660	0.00077
-2349	2453910.53966	0.00075
-2344	2453911.60580	0.00083
-2321	2453916.52289	0.00123
-2316	2453917.58959	0.00069
-2311	2453918.65917	0.00101
-2307	2453919.51645	0.00267
-2302	2453920.58170	0.00107
-2283	2453924.64256	0.00080
-2237	2453934.47576	0.00267
-2232	2453935.53884	0.00072
-2227	2453936.60849	0.00056
-2199	2453942.59180	0.00267
-2195	2453943.44516	0.00267
-2190	2453944.51297	0.00267
-2148	2453953.48793	0.00040
-2143	2453954.55777	0.00077
-2115	2453960.53955	0.00067
-2111	2453961.39629	0.00093
-2097	2453964.38780	0.00053
-2092	2453965.45552	0.00037
-2050	2453974.42931	0.00040
-2045	2453975.49880	0.00051
-2031	2453978.48999	0.00045
-2027	2453979.34570	0.00077
-2008	2453983.40481	0.00104
-1985	2453988.31864	0.00267
-1980	2453989.38704	0.00072
-1961	2453993.44873	0.00134
-1947	2453996.44038	0.00267
-1943	2453997.29469	0.00267
-1933	2453999.43164	0.00053
-1929	2454000.28576	0.00067
-1924	2454001.35314	0.00099
-1919	2454002.42266	0.00254
-1915	2454003.27746	0.00053
-1901	2454006.26940	0.00075
-1896	2454007.33783	0.00075
-1891	2454008.40794	0.00142
-1825	2454022.50757	0.00080
-1797	2454028.49182	0.00059
-1788	2454030.41738	0.00267
-1784	2454031.27006	0.00267
-1779	2454032.33882	0.00061
-1765	2454035.33068	0.00056
-1760	2454036.39877	0.00115
-1756	2454037.25197	0.00085
-1751	2454038.32308	0.00080
-1718	2454045.37236	0.00118
-1713	2454046.44185	0.00069
-1709	2454047.29360	0.00267
-1695	2454050.28889	0.00147

Table 2. continued.

Epoch	Heliocentric Julian Date	Uncertainty (days)
-1676	2454054.34772	0.00067
-673	2454268.66929	0.00267
-664	2454270.59202	0.00093
-659	2454271.66180	0.00123
-650	2454273.58502	0.00048
-645	2454274.65293	0.00037
-598	2454284.70093	0.00032
-584	2454287.68879	0.00267
-580	2454288.54254	0.00267
-561	2454292.60289	0.00075
-552	2454294.52532	0.00043
-547	2454295.59421	0.00053
-542	2454296.66176	0.00080
-538	2454297.51815	0.00267
-533	2454298.58606	0.00072
-528	2454299.65271	0.00091
-524	2454300.50250	0.00267
-519	2454301.57873	0.00134
-505	2454304.56864	0.00083
-384	2454330.42290	0.00101
-379	2454331.49316	0.00099
-374	2454332.55956	0.00045
-370	2454333.41443	0.00061
-365	2454334.48354	0.00048
-346	2454338.54382	0.00064
-318	2454344.52434	0.00267
-309	2454346.44888	0.00061
-300	2454348.37196	0.00075
-290	2454350.50762	0.00069
-286	2454351.36289	0.00067
-281	2454352.43173	0.00061
-276	2454353.50031	0.00045
-272	2454354.35412	0.00048
-258	2454357.34597	0.00267
-244	2454360.33693	0.00045
-239	2454361.40646	0.00048
-234	2454362.47410	0.00101
-230	2454363.32844	0.00085
-225	2454364.39655	0.00077
-220	2454365.46480	0.00128
-188	2454372.30561	0.00267
-160	2454378.28677	0.00061
-155	2454379.35438	0.00051
-127	2454385.33677	0.00208
-122	2454386.40601	0.00059
-118	2454387.26227	0.00123
-108	2454389.39839	0.00048
-103	2454390.46666	0.00099
-99	2454391.31929	0.00083
-94	2454392.39075	0.00152
-89	2454393.45708	0.00069
-66	2454398.37012	0.00267
-61	2454399.44210	0.00267
-33	2454405.42300	0.00208
-29	2454406.27824	0.00184
-24	2454407.34657	0.00267
-10	2454410.33193	0.00534
-5	2454411.40659	0.00104
0	2454412.47430	0.00093
4	2454413.33004	0.00222

Table 2. continued.

Epoch	Heliocentric Julian Date	Uncertainty (days)
9	2454414.39831	0.00088
14	2454415.46708	0.00267
18	2454416.31957	0.00267
23	2454417.39073	0.00101
28	2454418.45679	0.00267
42	2454421.45036	0.00267
46	2454422.30272	0.00048
51	2454423.37228	0.00120
56	2454424.44301	0.00120
60	2454425.29264	0.00104
79	2454429.35473	0.00134
93	2454432.34553	0.00101
98	2454433.42021	0.00096
1105	2454648.58473	0.00096
1110	2454649.65321	0.00267
1161	2454660.54641	0.00099
1166	2454661.61721	0.00267
1180	2454664.61213	0.00267
1189	2454666.53495	0.00101
1194	2454667.60021	0.00267
1217	2454672.51604	0.00310
1222	2454673.58436	0.00171
1227	2454674.65122	0.00112
1236	2454676.57263	0.00267
1241	2454677.64389	0.00184
1245	2454678.49766	0.00134
1269	2454683.62471	0.00163
1273	2454684.48023	0.00123
1278	2454685.55084	0.00254
1283	2454686.62008	0.00155
1287	2454687.47046	0.00171
1292	2454688.53802	0.00267
1297	2454689.60880	0.00083
1301	2454690.46396	0.00147
1306	2454691.53129	0.00184
1353	2454701.57659	0.00267
1371	2454705.42150	0.00126
1409	2454713.54132	0.00150
1413	2454714.39318	0.00101
1418	2454715.46511	0.00259
1423	2454716.52846	0.00534
1446	2454721.44473	0.00096
1451	2454722.51393	0.00126
1488	2454730.41819	0.00174
1493	2454731.48987	0.00112
1497	2454732.34311	0.00267
1507	2454734.47645	0.00195
1511	2454735.33269	0.00168
1521	2454737.46938	0.00206
1525	2454738.32459	0.00267
1535	2454740.46443	0.00101
1549	2454743.45446	0.00139
1553	2454744.30939	0.00139
1558	2454745.37454	0.00171
1563	2454746.44635	0.00267
1577	2454749.43736	0.00088
1614	2454757.34004	0.00085
1619	2454758.41305	0.00267
1623	2454759.26587	0.00267
1637	2454762.25622	0.00123

Table 2. continued.

Epoch	Heliocentric Julian Date	Uncertainty (days)
1642	2454763.32609	0.00144
1647	2454764.39387	0.00187
1652	2454765.45763	0.00206
1656	2454766.31757	0.00184
1661	2454767.38690	0.00110
1666	2454768.45102	0.00267
1675	2454770.37485	0.00267
1680	2454771.44470	0.00112
1684	2454772.30295	0.00267
1694	2454774.43463	0.00200
1698	2454775.28986	0.00147
1750	2454786.40225	0.00152
2799	2455010.54183	0.00286
2809	2455012.68445	0.00267
2813	2455013.53607	0.00224
2818	2455014.60170	0.00534
2851	2455021.65333	0.00267
2855	2455022.50561	0.00126
2888	2455029.56044	0.00288
2893	2455030.62470	0.00267
2897	2455031.48286	0.00267
2902	2455032.55379	0.00112
2907	2455033.61997	0.00267
2911	2455034.47662	0.00267
2925	2455037.46840	0.00110
2930	2455038.53667	0.00131
2935	2455039.60552	0.00304
2940	2455040.66175	0.00224
2963	2455045.59261	0.00136
2967	2455046.43898	0.00123
2972	2455047.51171	0.00176
3019	2455057.55330	0.00267
3023	2455058.41182	0.00801
3028	2455059.47648	0.00179
3033	2455060.54497	0.00534
3038	2455061.61446	0.00267
3051	2455064.38493	0.00085
3056	2455065.46223	0.00174
3061	2455066.52331	0.00267
3065	2455067.38210	0.00267
3070	2455068.45596	0.00534
3084	2455071.44529	0.00321
3094	2455073.57723	0.00136
3098	2455074.43122	0.00219
3103	2455075.49689	0.01068
3149	2455085.32602	0.00147
3173	2455090.46059	0.00160
3187	2455093.44727	0.00267
3205	2455097.29448	0.00072
3271	2455111.40251	0.00339
3280	2455113.31981	0.00136
3285	2455114.39646	0.00131
3304	2455118.45370	0.00248
3308	2455119.30761	0.00158
3318	2455121.43799	0.00267
3322	2455122.29840	0.00168
3327	2455123.36042	0.00267
3332	2455124.42853	0.00267
3346	2455127.42506	0.00267
3350	2455128.27909	0.00534

Table 2. continued.

Epoch	Heliocentric Julian Date	Uncertainty (days)
3411	2455141.31090	0.00211
3416	2455142.38037	0.00267
3453	2455150.29269	0.00267
3463	2455152.42755	0.00155
3467	2455153.28229	0.00534
6183	2455733.65438	0.00534
6216	2455740.69178	0.00101
6262	2455750.50511	0.00534
6267	2455751.59120	0.00534
6272	2455752.65743	0.00267
6276	2455753.49949	0.01068
6286	2455755.66517	0.00267
6290	2455756.48744	0.00801
6295	2455757.56952	0.00278
6300	2455758.64359	0.01068
6304	2455759.49594	0.00801
6309	2455760.56053	0.00150
6314	2455761.63443	0.00267
6318	2455762.48263	0.00534
6323	2455763.55964	0.00267
6328	2455764.63517	0.00801
6332	2455765.47635	0.00166
6365	2455772.53046	0.00128
6370	2455773.59822	0.00267
6374	2455774.44192	0.01068
6379	2455775.53433	0.00801
8793	2456291.33132	0.00069